International Communications in Heat and Mass Transfer 81 (2017) 218–228

Contents lists available at ScienceDirect

International Communications in Heat and Mass Transfer

journal homepage: www.elsevier.com/locate/ichmt

Unsteady conjugate natural convection in a porous cavity boarded by two vertical finite thickness walls

H. Zargartalebi [a], M. Ghalambaz [b], K. Khanafer [c,d,*], I. Pop [e]

[a] Department of Mechanical Engineering, Shahid Chamran University of Ahvaz, Ahvaz, Iran
[b] Department of Mechanical Engineering, Dezful Branch, Islamic Azad University, Dezful, Iran
[c] Mechanical Engineering Department, Australian College of Kuwait, Kuwait, Safat 13060, Kuwait
[d] Department of Biomedical Engineering Department, University of Michigan, Ann Arbor, MI 48109, USA
[e] Department of Applied Mathematics, Babeş-Bolyai University, 400084 Cluj-Napoca, Romania

ARTICLE INFO

Available online xxxx

Keywords:
Porous media
Periodic boundary condition
Local thermal non-equilibrium
Conjugate natural convection

ABSTRACT

The objective of this study is to investigate unsteady conjugate natural convection in a porous cavity sandwiched by finite conductive walls considering time-periodic boundary conditions and local thermal non-equilibrium. The top and bottom boundaries are assumed to be isolated and the continuity of temperature and heat transfer are considered in interface boundaries. The effect of varying a plethora of parameters such as Rayleigh number, Thermal conductivity ratio, wall thickness, and non-dimensional frequency on the streamlines, isotherms, and Nusselt number has been studied. It is shown that, apart from non-dimensional frequency and wall thickness, the amplitude of periodic fluid Nusselt number is an increasing function of all aforementioned parameters. Furthermore, aside from Rayleigh number and heat transfer coefficient, the behavior of the solid Nusselt number is the same as fluid Nusselt number. Eventually, the time-averaged Nusselt number and heat transfer through the vertical walls for different values of non-dimensional frequencies are calculated.

1. Introduction

The phenomenon of convective heat transfer in a fluid-saturated porous medium has received considerable attention in the past few years due to its importance in various applications. Such applications include thermal insulation, biomedical engineering applications, drying processes, radioactive waste management, transpiration cooling, geophysical systems and contaminant transport in groundwater [1–7]. Comprehensive reviews of the existing studies on these topics can be found in monographs by Nield and Bejan [8], Vafai [9], AlAmiri [10], Ingham and Pop [11,12], and Pop and Ingham [13]. Conjugate natural convection in enclosures where heat conduction in a solid wall of finite thickness is coupled with heat convection in an adjacent fluid has been studied extensively in the literature [14–19]. Kim and Viskanta [14,15] analyzed experimentally and numerically the effects of wall conductance on natural convection in square enclosures. They found that heat conduction along the conducting adiabatic walls simultaneously stabilize and destabilize the fluid in the cavity. Meanwhile, conjugate natural convection in enclosures filled with porous media has received less attention. This type of configuration is of interest in several engineering applications. In particular, the solidification process in porous media and building insulation layers. AlAmiri et al. [16] addressed the wall heat conduction effect on the steady natural convection heat transfer within a two-dimensional cavity filled with a fluid-saturated porous medium. The generalized model of the momentum equation was used in representing the fluid motion inside the porous cavity. Their results showed that as the wall thickness increased, the temperature difference between the interface temperature and the cold boundary reduced. However, appreciated increase in the fluid circulation intensity within the porous medium was achieved when considering thin wall thickness, large wall-to-fluid thermal conductivity ratio and large aspect ratio values.

Sheremet and Pop [17] investigated steady-state natural convection heat transfer in a square porous cavity having solid walls of finite thickness and conductivity filled by a nanofluid. The authors formulated their equations in terms of voricity-stream function formulation. Their results illustrated that local Nusselt number at the solid-porous interface was an increasing function of Rayleigh number, buoyancy-ratio parameter and a decreasing function of thermophoresis parameter, Lewis number, and wall thickness. Conjugate natural convection-conduction heat transfer in a square enclosure with a finite-wall thickness was studied numerically by Saleh et al. [18]. The Darcy model was used in the mathematical formulation for the porous layer. It was found that the number of contrarotative cells and the strength circulation of each cell can be controlled by the thickness of the bottom wall, the thermal conductivity ratio and the Rayleigh number. It was also illustrated that increasing

* Corresponding author at: Mechanical Engineering Department, Australian College of Kuwait, Kuwait, Safat 13060, Kuwait.
E-mail address: k.khanafer@ack.edu.kw (K. Khanafer).

http://dx.doi.org/10.1016/j.icheatmasstransfer.2016.12.016
0735-1933/

Nomenclature

D	dimensionless wall thickness
f	dimensionless oscillating frequency
H	heat transfer coefficient parameter, defined in Eq. (6)
k	thermal conductivity (W m^{-1} K^{-1})
K	permeability of the porous medium (m^2)
K_r	thermal conductivity ratio parameter, defined in Eq. (6)
L	wall height (m)
Q_w	dimensionless heat transfer through the walls, Eq. (8)
Ra	Rayleigh number for porous medium, $=g\beta KT_hL/\varepsilon\nu\alpha_f$
R_k	wall to fluid thermal conductivity ratio, $=k_w/(\varepsilon k_f)$
t	Time (s)
T	temperature (K)
x, y	Cartesian coordinates (m)
X, Y	non-dimensional Cartesian coordinates

Greek symbols

α	effective thermal diffusivity (m^2 s^{-1})
β	coefficient of thermal expansion (K^{-1})
ε	Porosity
θ	non-dimensional temperature
υ	kinematic viscosity (m^2 s^{-1})
τ	non-dimensional time
ψ	stream function, $u=\partial\psi/\partial y$, $v=-\partial\psi/\partial x$
Ψ	non-dimensional stream function
ω	oscillating frequency

Subscripts

c	cold
f	fluid
h	hot
s	solid
w	wall

either Rayleigh number of the thermal conductivity ratio or both, and decreasing the thickness of the bounded wall increased the average Nusselt number of the porous enclosure. Varol et al. [19] studied entropy generation due to conjugate natural convection heat transfer and fluid flow inside an enclosure bounded by two solid massive walls from vertical sides at different thicknesses. The enclosure was assumed differentially heated from vertical walls and horizontal walls were adiabatic. It was found that entropy generation increased with increasing of thermal conductivity ratio and thicknesses of the walls. Moreover, entropy generation due to heat transfer was found more significant than that of fluid flow irreversibility for all values of thickness of the solid vertical walls.

One can notice from the above cited references that natural convection heat transfer in a porous cavity bounded by vertical walls of finite thickness under local non-thermal equilibrium received less attention in the literature. The main objective of the present work is to study the effect of varying Rayleigh number, Thermal conductivity ratio, wall thickness, and non-dimensional frequency on the streamlines, isotherms, and Nusselt number under local non-thermal equilibrium condition.

2. Mathematical formulation

Consider a two-dimensional unsteady, incompressible natural convection in a porous cavity sandwiched between two equal thickness walls. The porous enclosure is considered to be local thermal non-equilibrium with symmetric boundary conditions in top and bottom horizontal boundaries. Due to no-slip boundary condition the velocity magnitude on the walls is equal to zero. Moreover, the right boundary condition has a constant temperature and the left temperature boundary condition fluctuates with a sinusoidal function. The solid walls are considered to be rigid and impermeable. Apart from density variation in the buoyancy force which conformed to Boussinesq approximation, the other physical properties of the fluid are considered to be constant. A schematic of the physical domain is represented in Fig. 1. In order to capture the necessary gradients, a non-uniform mesh is utilized which is clustered near the boundaries. The governing equations comprising momentum and energy are represented for fluid and solid here in canonical forms as derived by several researchers [8,9,11–12]:

$$\frac{\partial^2\Psi}{\partial X^2}+\frac{\partial^2\Psi}{\partial Y^2}=-Ra\frac{\partial\theta_f}{\partial Y} \tag{1}$$

$$\frac{\partial\theta_f}{\partial\tau}+\frac{\partial\Psi}{\partial Y}\frac{\partial\theta_f}{\partial X}-\frac{\partial\Psi}{\partial X}\frac{\partial\theta_f}{\partial Y}=\frac{\partial^2\theta_f}{\partial X^2}+\frac{\partial^2\theta_f}{\partial Y^2}+H(\theta_s-\theta_f) \tag{2}$$

$$\frac{\partial\theta_s}{\partial\tau}=\frac{\partial^2\theta_s}{\partial X^2}+\frac{\partial^2\theta_s}{\partial Y^2}+HK_r(\theta_f-\theta_s) \tag{3}$$

$$\frac{\partial\theta_w}{\partial\tau}=\frac{\partial^2\theta_w}{\partial X^2}+\frac{\partial^2\theta_w}{\partial Y^2} \tag{4}$$

Eqs. (1)–(4) are nondimensionalized utilizing the ensuing variables:

$$\tau=\frac{\varepsilon\alpha_f t}{L^2}\ ,\quad X=\frac{x}{L}\ ,\quad Y=\frac{y}{L}\ ,\quad \mathrm{D}=\frac{d}{L}\ ,\quad \theta=\frac{T-T_c}{T_h}\ ,\quad \Psi=\frac{\psi}{\varepsilon\alpha_f} \tag{5}$$

where parameters arising in dimensionless Eqs. (1)–(4) can be expressed as:

$$Ra=\frac{g\beta KT_hL}{\varepsilon\nu\alpha_f}\ ,\quad H=\frac{h_{fs}L^2}{\varepsilon k_f}\ ,\quad K_r=\frac{\varepsilon k_f}{(1-\varepsilon)k_s} \tag{6}$$

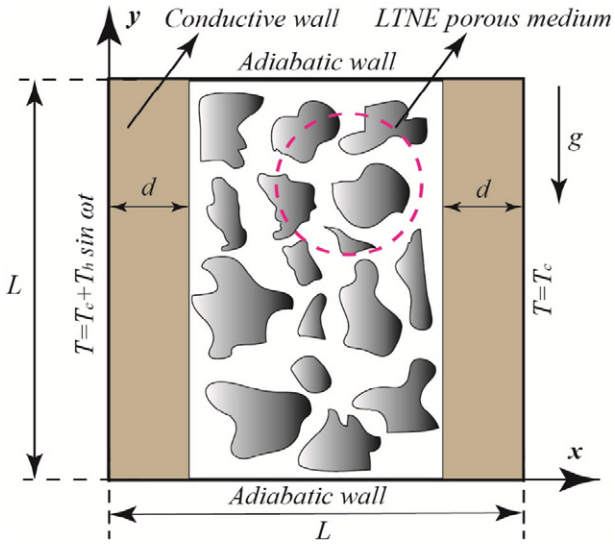

Fig. 1. Schematic diagram of coordinate system and physical model.

The above equations are subjected to the following initial and boundary conditions:

$$\begin{aligned}
&\Psi(X,Y,0)=0,\ \theta_f(X,Y,0)=\theta_w(X,Y,0)=\theta_s(X,Y,0)=0.5\\
&\theta_w(0,Y,\tau)=\ sin f\tau\ ,\ \theta_w(1,Y,\tau)=0\\
&\Psi(X,0,\tau)=0\ ,\quad \frac{\partial\theta_f(X,0,\tau)}{\partial Y}=\frac{\partial\theta_w(X,0,\tau)}{\partial Y}=\frac{\partial\theta_s(X,0,\tau)}{\partial Y}=0\\
&\Psi(X,1,\tau)=0\ ,\quad \frac{\partial\theta_f(X,1,\tau)}{\partial Y}=\frac{\partial\theta_p(X,1,\tau)}{\partial Y}=\frac{\partial\theta_s(X,1,\tau)}{\partial Y}=0\\
&\Psi(D,Y,\tau)=0\ ,\ \theta_w(D,Y,\tau)=\theta_f(D,Y,\tau)=\theta_s(D,Y,\tau)\\
&\Psi(1-D,Y,\tau)=0\ ,\ \theta_w(1-D,Y,\tau)=\theta_f(1-D,Y,\tau)=\theta_s(1-D,Y,\tau)\\
&\frac{\partial\theta_f(D,Y,\tau)}{\partial X}=R_k\frac{\partial\theta_w(D,Y,\tau)}{\partial X}-\frac{1}{k_r}\frac{\partial\theta_s(D,Y,\tau)}{\partial X}\\
&\frac{\partial\theta_f(1-D,Y,\tau)}{\partial X}=R_k\frac{\partial\theta_w(1-D,Y,\tau)}{\partial X}-\frac{1}{k_r}\frac{\partial\theta_s(1-D,Y,\tau)}{\partial X}
\end{aligned}\tag{7}$$

where $f=(\omega L^2)/(\varepsilon\alpha_f)$ denotes dimensionless oscillating frequency and $R_k=k_w/(\varepsilon k_f)$ is the wall to fluid thermal conductivity ratio. Furthermore, the physical quantities of interest in this study are heat transfer through the walls and fluid and solid Nusselt numbers, respectively, as follows:

$$\begin{aligned}
Q_w&=-\int_0^1\frac{\partial\theta_w}{\partial X}\Big|_{X=0,1}dY,\\
Nu_f&=-\int_0^1\frac{\partial\theta_f}{\partial X}\Big|_{X=D,1-D}dY,\\
Nu_s&=-\int_0^1\frac{\partial\theta_s}{\partial X}\Big|_{X=D,1-D}dY
\end{aligned}\tag{8}$$

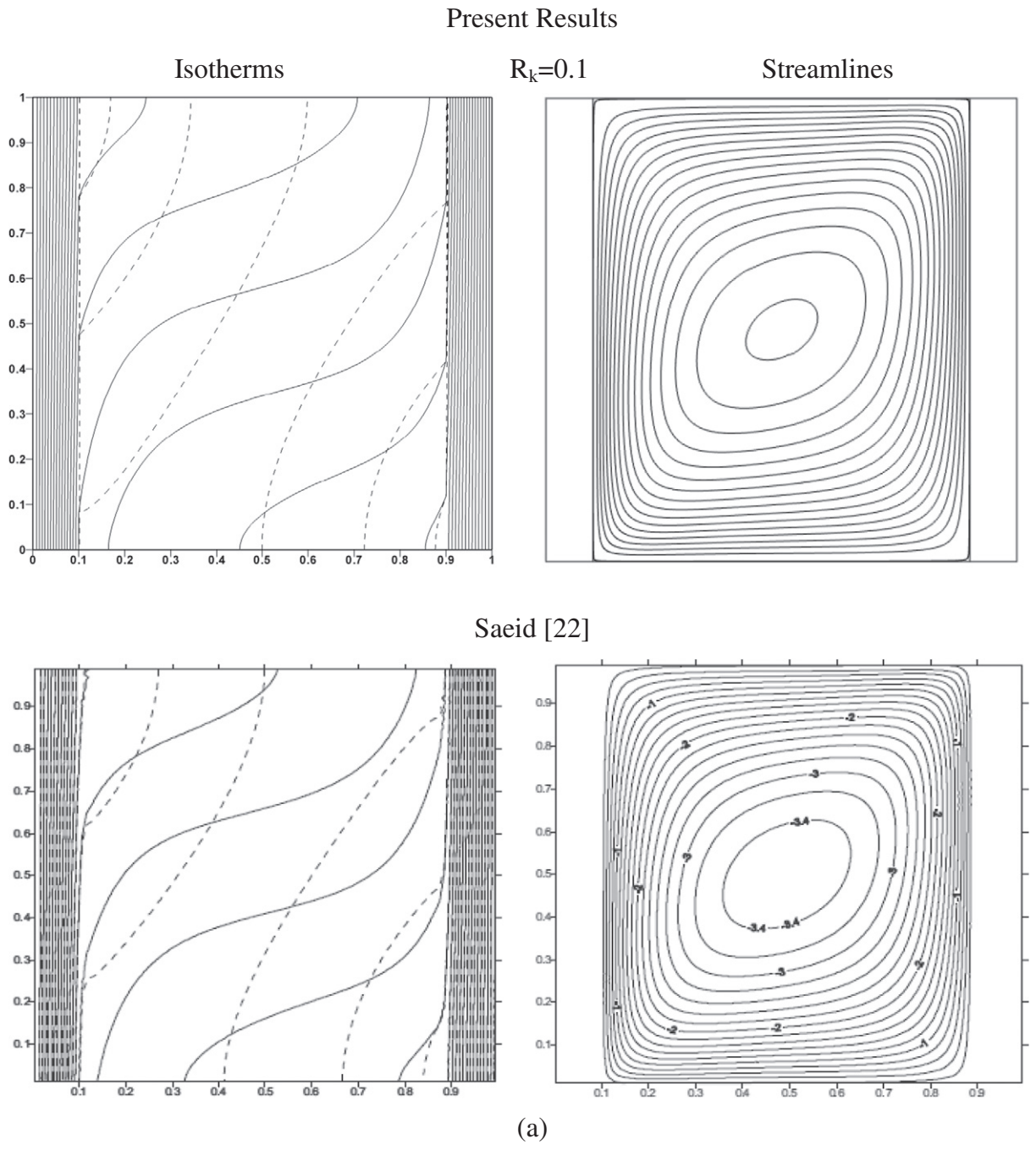

Fig. 2. Comparison of the isotherms (solid line for θ_f, dashed line for θ_s) and streamlines between present results and Saeid [22] at $Ra=10^3$, $D=01$, $k_r=1$, and $H=1$: (a) $R_k=0.1$, (b) $R_k=1$, (c) $R_k=10$.

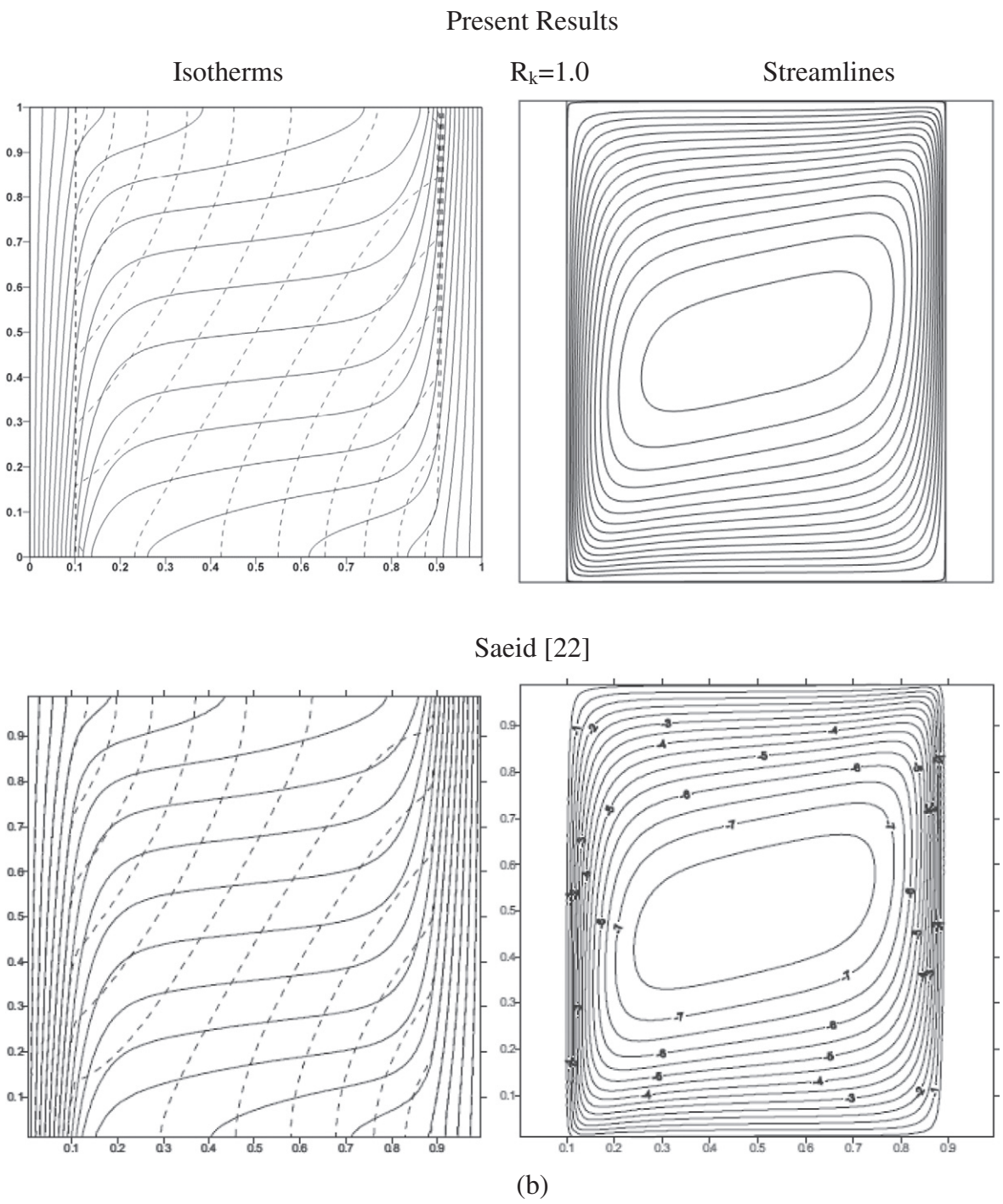

Fig. 2 (*continued*).

The time-averaged heat transfer through the walls and Nusselt numbers is given by:

$$\overline{Q}_w = -\frac{f}{2\pi}\int_0^{2\pi/f}\int_0^1 \left.\frac{\partial\theta_w}{\partial X}\right|_{X=0,1} dY d\tau$$
$$\overline{Nu}_f = -\frac{f}{2\pi}\int_0^{2\pi/f}\int_0^1 \left.\frac{\partial\theta_f}{\partial X}\right|_{X=D,1-D} dY d\tau \quad (9)$$
$$\overline{Nu}_s = -\frac{f}{2\pi}\int_0^{2\pi/f}\int_0^1 \left.\frac{\partial\theta_s}{\partial X}\right|_{X=D,1-D} dY d\tau$$

3. Method of solution and validation

The system of partial differential, Eqs. (1)–(4), along with the boundary conditions, Eq. (7), is transformed to a weak form and solved numerically utilizing the Galerkin finite-element method with iteration. The iteration process terminates when the residuals for the defined dependent variables become lower than 10^{-8}. The detailed solution method can be found in the previous studies [20,21]. In order to confirm the solution procedure validation, the problem introduced by Saied [22] in which a porous cavity horizontally sandwiched between two conductive walls and is adiabatic at top and bottom boundaries is solved numerically. The left and right vertical walls are considered to have

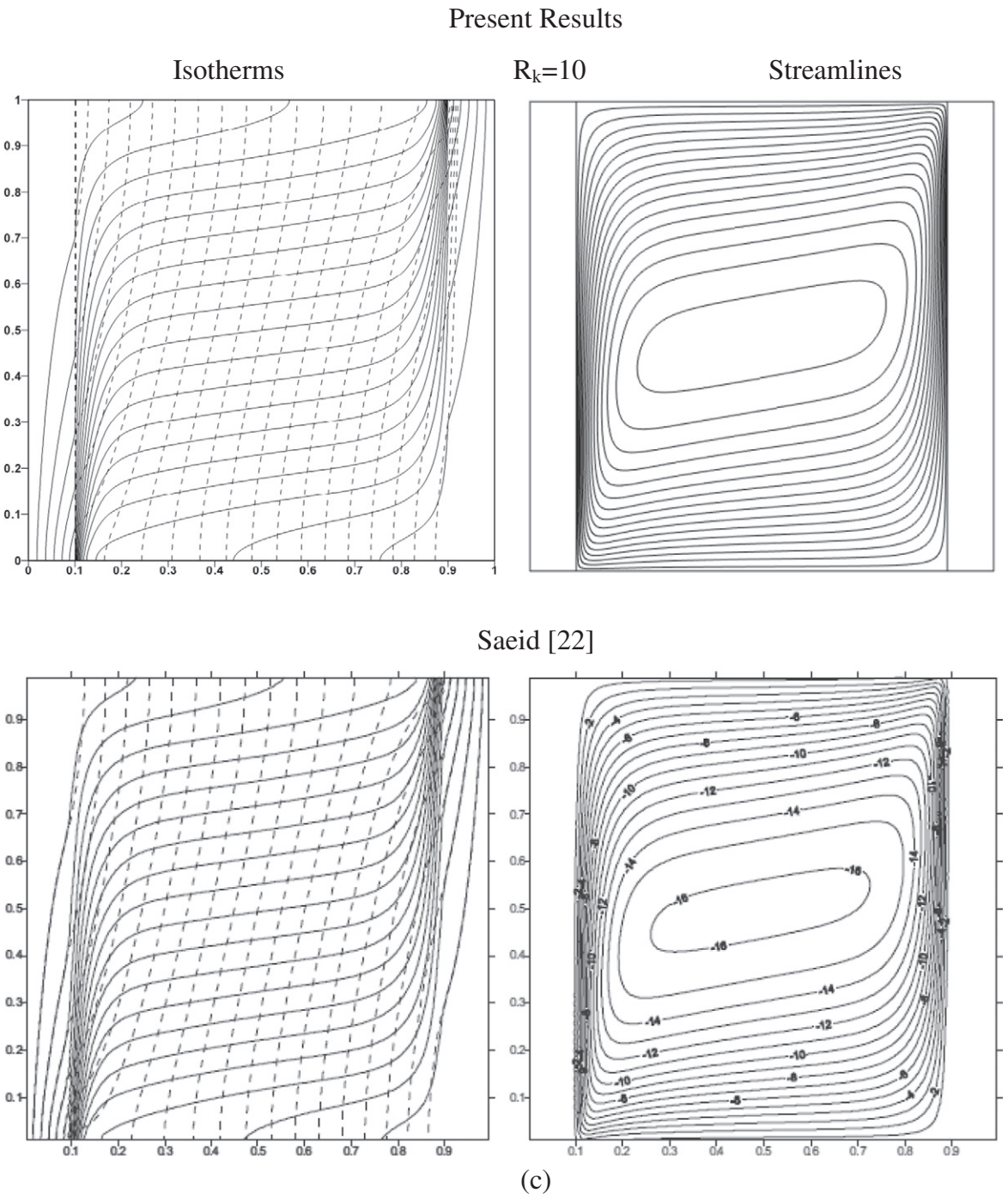

Fig. 2 (*continued*).

constant temperatures T_h and T_c respectively. In addition, the porous structure is in local thermal non-equilibrium condition. The streamlines and isotherms for different values of R_k are compared with Saeid results in Fig. 2. Moreover, the variation of average Nusselt numbers with R_k is compared by the results of the Saeid [22] in Fig. 3. It is shown that the results, computed in the present study, are in excellent agreement with the results reported in the literature [22].

4. Results and discussion

The isotherms and streamlines of the free convection flow for 9th period, in which the flow and heat transfer is fully-developed, are depicted in Figs. 4 and 5. The constant parameters are considered to be $Ra = 10^3$, $D = 0.1$, $f = 10\pi$, $K_r = H = R_k = 1$. According to subplots (a)-(h) in Fig. 4, the isotherms distribution is affected by the sinusoidal themperature value of the left wall. In essence, varying the left wall temperature influences the bouyancy force and leads to periodic change of the solid and fluid temperature distributions. As an illustration, comparing the subplots (c) and (g), in which the dimensionless time is equal to 1.65 and 1.75 respectively, due to the value of left wall temperature, the isotherms are placed in opposite positions with respect to each other.

In accordance with Fig. 5, the direction of the streamlines is majorly affected by the sinusoidal variation of the left wall temperature. As an illustration, in subplots (b)-(d), in which the magnitude of temperature

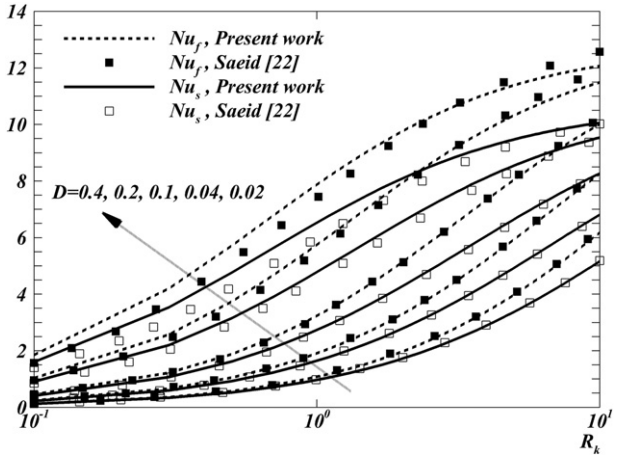

Fig. 3. Variation of average Nu_f and Nu_s with R_k for different values of D and fixed $Ra = 10^3$, $D = 0.1$, $R_k = 0.1$, $K_r = H = 100$.

in the left vertical wall is positive and the periodic temperature is in first half of its period, the clockwise circulation in the left down corner of the enclosure is gradually generated and becomes greater and eventually encompasses the cavity. On the other hand, in the second half of the period (subplots (*f*)-(*a*)) in which the left wall temperature becomes negative, a counter clockwise circulation is generated from the left up corner of the cavity. Furthermore, some small cells in the cavity appeared due to the oscillation of the left temperature boundary condition in which the buoyancy force in the different parts of the cavity has a sinusoidal behavior.

The influence of non-dimensional frequency on solid and fluid Nusselt numbers and heat transfer through the walls is represented in Figs. 6 and 7. As it is seen in Fig. 4, the magnitude of both Nusselt numbers oscillates during the time. Moreover, the amplitude of the swinging function is decreased as the value of the non-dimensional frequency increases. In other words, the effect of varying left wall temperature on the temperature of the interior domain significantly dwindles by augmenting the non-dimensional frequency. On the other hand, the heat

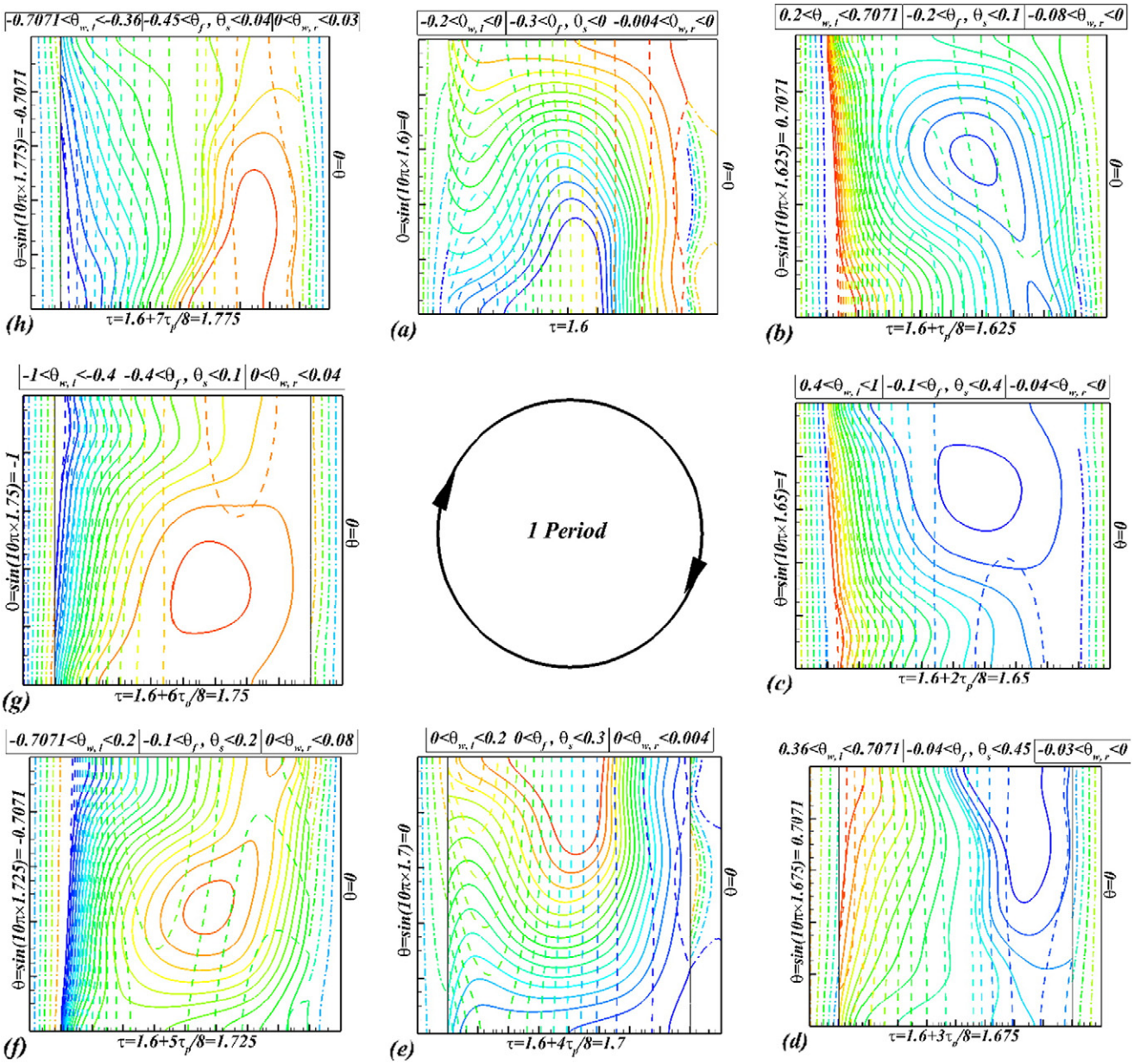

Fig. 4. Sequential plots of isotherms for a period of oscillations; $Ra = 10^4$, $D = 0.1$, $f = 10\pi$, $K_r = H = R_k = 1$; solid line: fluid phase, dashed line: solid phase, and dash dot line: solid wall.

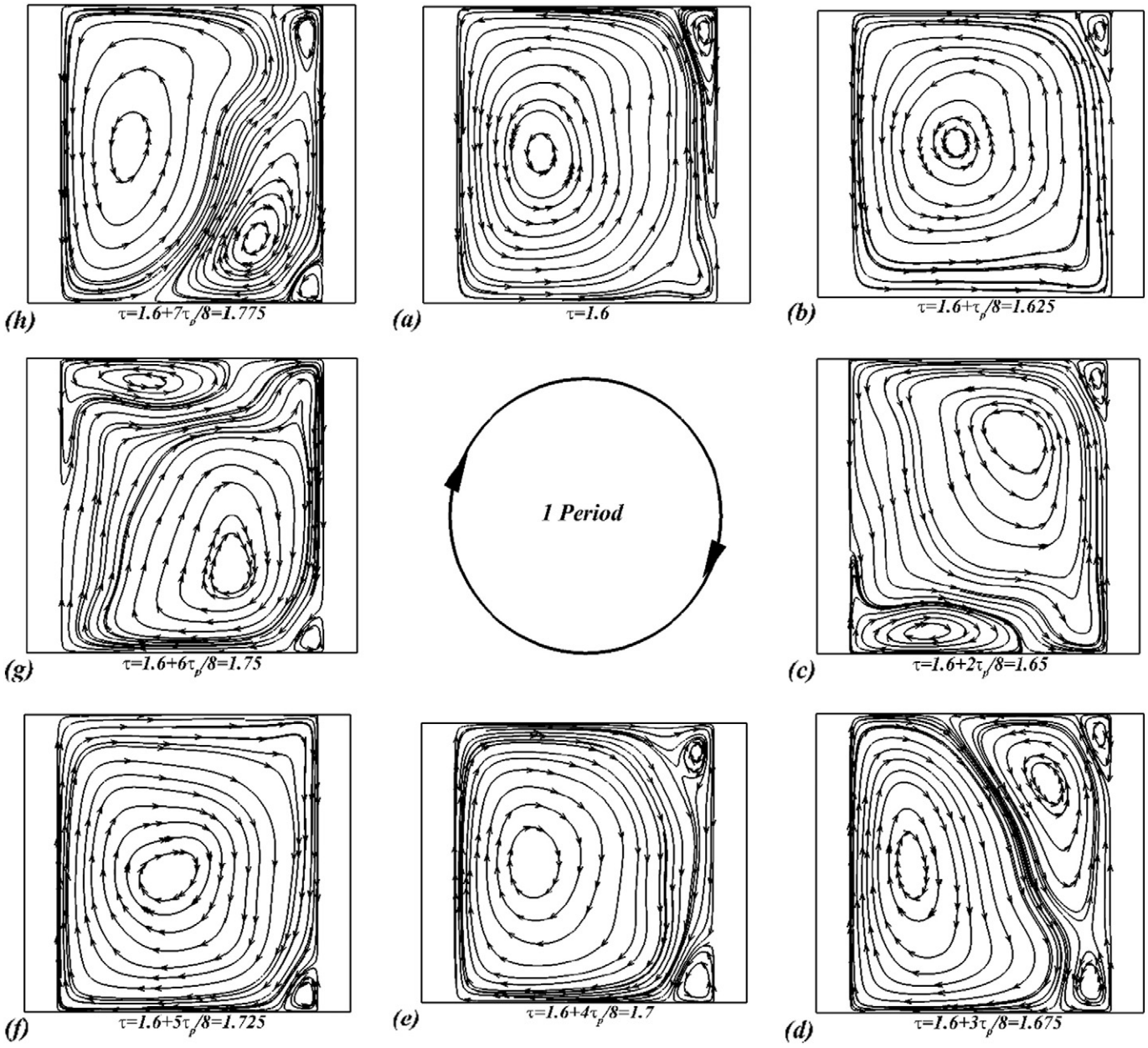

Fig. 5. Sequential plots of streamlines for a period of oscillations; $Ra = 10^4$, $D = 0.1$, $f = 10\pi$, $K_r = H = R_k = 1$.

transfer through the walls has a reverse behavior with respect to the Nusselt numbers. It means that the amplitude of the heat transfer through the walls is an increasing function of non-dimensional frequency.

It is worth mentioning here that the variation of Ra and K_r does not have tangible impact on the heat transfer through the walls; therefore, it has not been shown for the sake of brevity. The effect of variation of K_r on the solid and fluid Nusselt numbers is shown in Fig. 8. The results depict that the augmentation of K_r leads the amplitude of both Nusselt numbers to increase. Moreover, it is obvious that the variation of K_r has more influence on the Nu_s with respect to Nu_f. In essence, the more value of K_r increases, the more the magnitude of porosity soars. Therefore, the convective heat transfer becomes larger than the conductive heat transfer, i.e. the absolute value of both Nusselt numbers goes up significantly.

The solid and fluid Nusselt numbers for multifarious values of the Rayleigh numbers are represented in Fig. 9. It is shown that increasing of Ra causes the absolute value of the Nu_f to augment and the absolute value of Nu_s to decline respectively. In fact, augmentation of Rayleigh number induces dominating convective heat transfer than conductive heat transfer and as a consequence it leads to increase of dimensionless fluid temperature gradient and decrease of solid temperature gradient respectively. Further, in high values of Ra the function of solid and fluid Nusselt numbers deviates from the conventional sinusoidal from particularly in peaks.

The Nu_f, Nu_s, and Q_w for different values of wall to fluid thermal conductivity parameter (R_k) are represented in Figs. 10 and 11. As it is indicated, in contrast with heat transfer through the walls, the absolute magnitudes of the Nusselt numbers are increasing with the augmentation of the R_k. In addition, in high values of the R_k, the variation of this

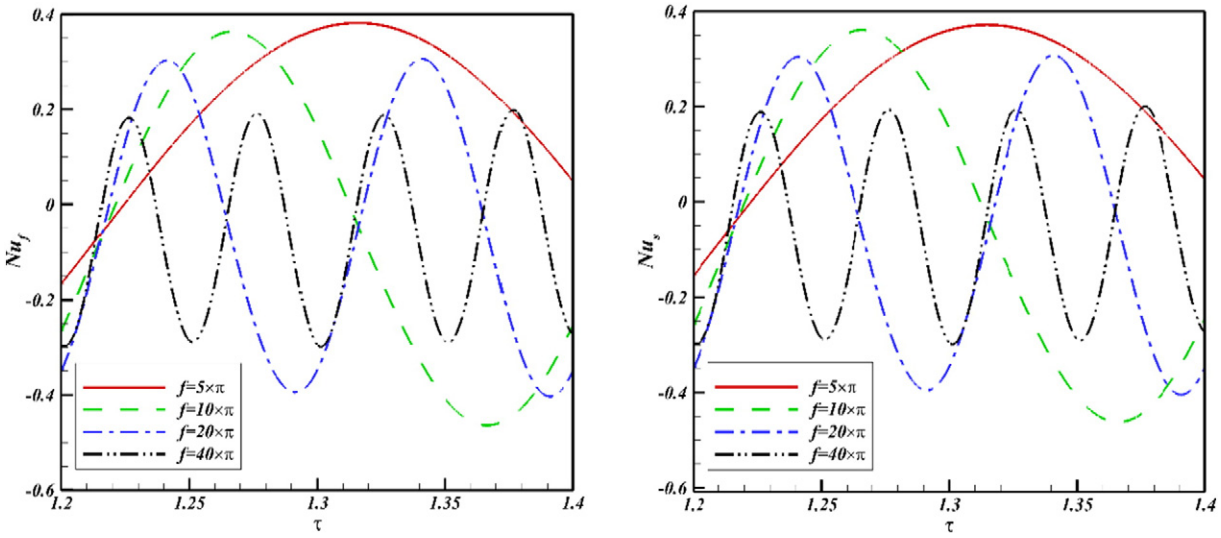

Fig. 6. The effect of non-dimensional frequency on fluid (left) and solid (right) Nusselt numbers of the left wall; $Ra = 10^3$, $D = 0.1$, $R_k = 0.1$, $K_r = H = 1$.

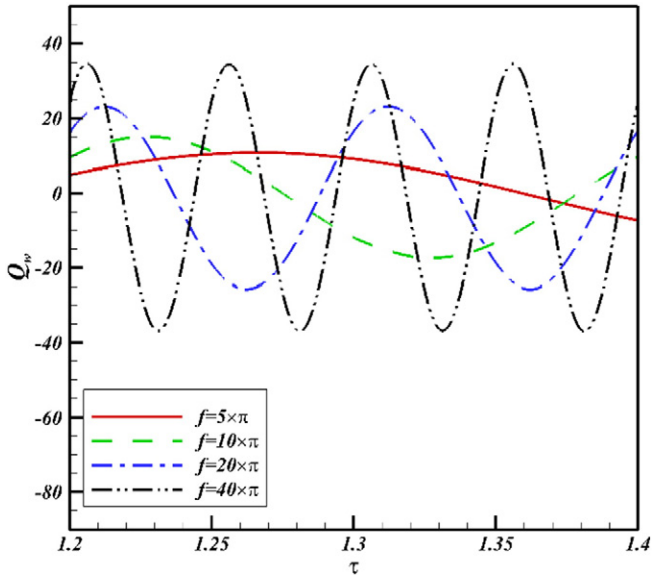

Fig. 7. The effect of non-dimensional frequency on heat transfer through the left wall; $Ra = 10^3$, $D = 0.1$, $R_k = 0.1$, $K_r = H = 1$.

parameter does not have considerable effect on the Nusselt numbers and Q_w. The variation of Nu_f, Nu_s, and Q_w with time for various values of the parameter D is shown in Figs. 12 and 13. As it is indicated, increase in wall thickness leads the absolute value of Nusselt numbers to decrease. In essence, the augmentation of the wall thickness induces dominating conductive heat transfer with respect to the convective one. Moreover, as depicted in Fig. 13, for the case which the thickness of the wall is thin ($D = 0.05$), the absolute value of Q_w is higher than other cases in contrast to the case in which $D = 0.1$. The absolute value of Q_w for the cases in which $D = 0.1$ and $D = 0.2$ placed in the middle of two former cases ($D = 0.05$, $D = 0.1$).

The effect of variation of heat transfer coefficient parameter (H) on the Nusselt numbers and Q_w is depicted in Figs. 14 and 15. The results show that in contrast with solid Nusselt number, increasing parameter H leads to increase the absolute values of the fluid Nusselt number and Q_w. It is worth mentioning that when the order of magnitude of the thermal conductivity ratio (K_r) is zero the variation of parameter H does not have significant influence on Nu_s, Nu_f, and Q_w. Moreover, it is represented that for the variables Nu_f and Q_w the cases which there is local thermal equilibrium and $H = 1$ are the same. On the other hand, regardless of the sign of value Nu_s, this value for LTE case is lower than the state in which $H = 1$. This means that the

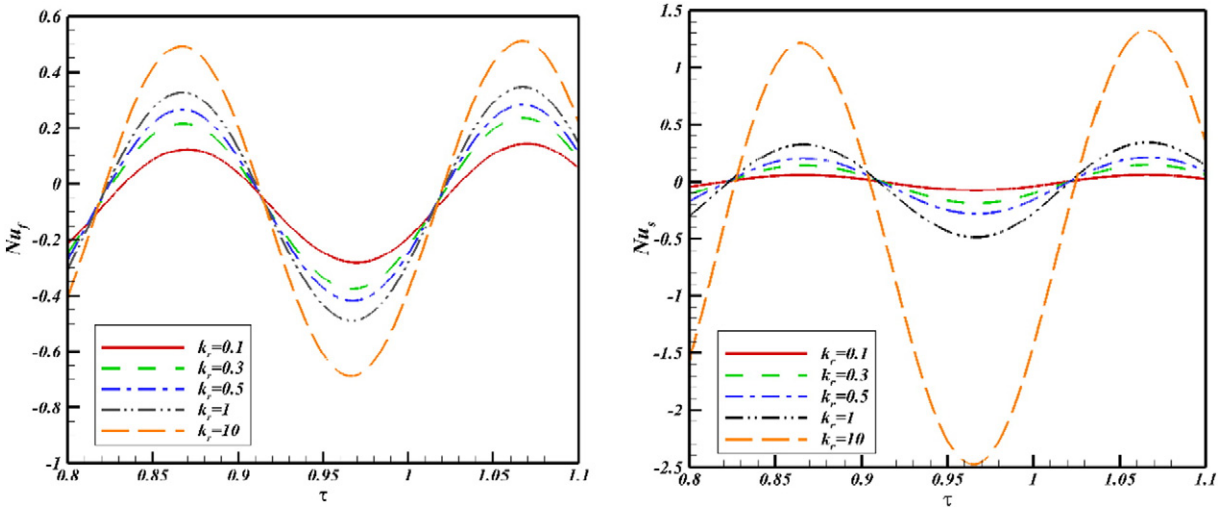

Fig. 8. The effect of K_r on fluid (left) and solid (right) Nusselt numbers of the left wall; $Ra = 10^3$, $D = 0.1$, $f = 10\pi$, $R_k = 0.1$, $H = 1$.

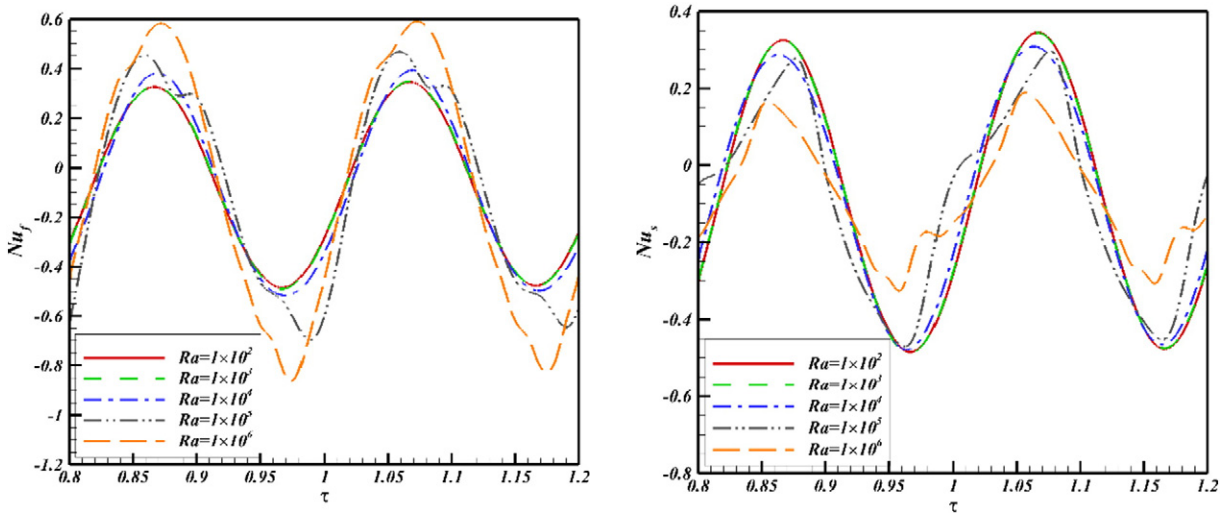

Fig. 9. The effect of Rayleigh number on fluid (left) and solid (right) Nusselt numbers of the left wall; $D = 0.1$, $f = 10\pi$, $R_k = 0.1$, $K_r = H = 1$.

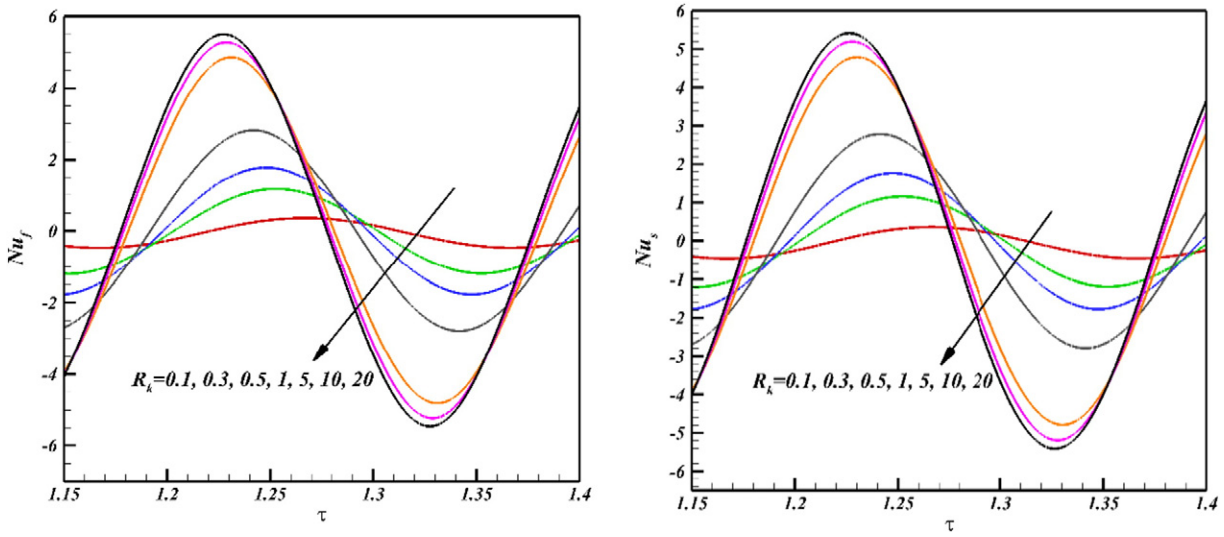

Fig. 10. The effect of R_k on fluid (left) and SOLID (right) Nusselt numbers of the left wall; $Ra = 10^3$, $D = 0.1$, $f = 10\pi$, $K_r = H = 1$.

time-averaged solid Nusselt number for LTE case is lower than the state in which $H = 1$.

Eventually, in order to evaluate the time-averaged parameters, the influence of non-dimensional frequency on the time-averaged Nusselt numbers and heat transfer through the walls is shown in Table 1. In accordance with Table 1, the parameter $\overline{Q}_w$ is an increasing function of the non-dimensional frequency. On the other hand, the values of parameters $\overline{Nu}_f$ and $\overline{Nu}_s$ are dwindled at $f = 30$ and afterwards slightly augment up to $f = 130$ and finally faced with a reduction in $f = 150$. In fact, the increase of dimensionless frequency affects the thermal stress of the solid walls and consequently, leads to change more in $\overline{Q}_w$ and less in $\overline{Nu}_f$ and $\overline{Nu}_s$.

5. Conclusions

The unsteady conjugate free convection in a porous medium enclosure placed between two conductive finite walls is studied. The left thermal boundary condition is assumed to be a periodic function of time and the right one is T_c. Moreover, the horizontal up and bottom walls are isolated. It is depicted that the heat transfer through the

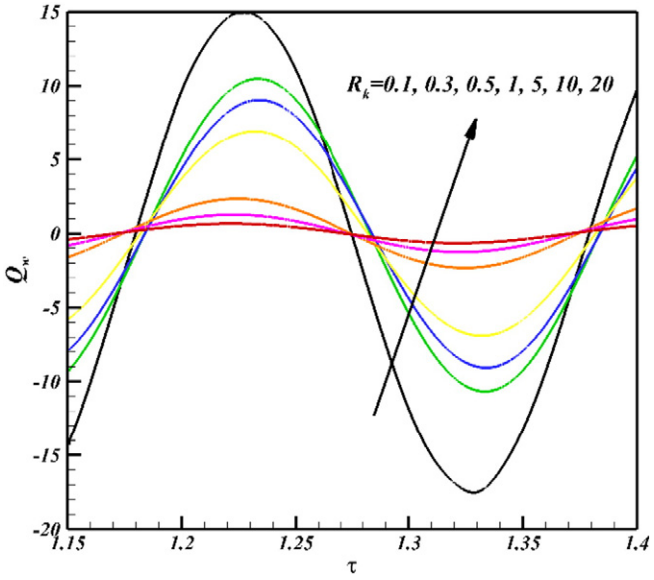

Fig. 11. The effect of R_k on heat transfer through the left wall; $Ra = 10^3$, $D = 0.1$, $f = 10\pi$, $K_r = H = 1$.

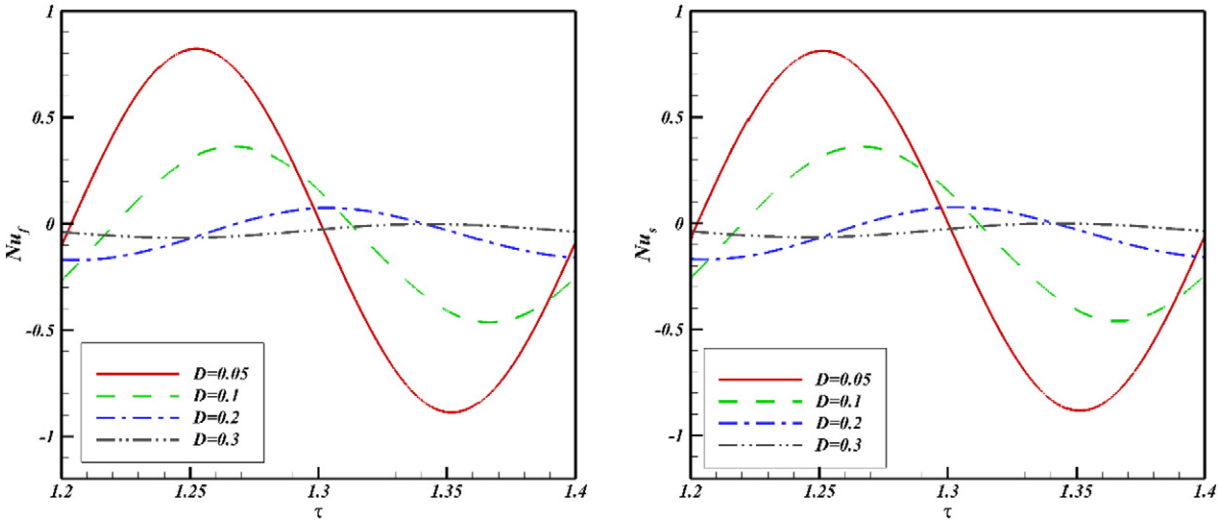

Fig. 12. The effect of parameter D on fluid (left) and solid (right) Nusselt numbers of the left wall; $Ra = 10^3$, $R_k = 0.1$, $f = 10\pi$, $K_r = H = 1$.

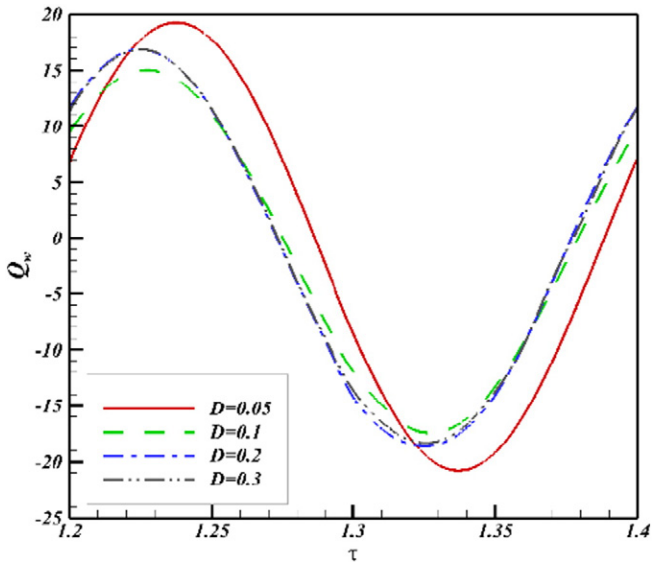

Fig. 13. The effect of parameter D on heat transfer through the left wall; $Ra = 10^3$, $R_k = 0.1$, $f = 10\pi$, $K_r = H = 1$.

vertical walls and Nusselt numbers are affected by left thermal boundary condition and have a periodic behavior along with time. In addition, the streamlines and isotherms have a periodical pattern as well. Contrary to heat transfer through the walls, the absolute Nusselt numbers increase as the non-dimensional frequency declines. Moreover, increase of K_r and R_k leads the amplitude of Nusselt numbers to augment. Also, it is found that the absolute Nusselt numbers magnitude is in reverse proportion with the thickness of the vertical walls. Further, in contrast with Nu_s, the more increase of Rayleigh number and parameter H, the more increase in Nu_f amplitude. Finally, it is shown that time-averaged Nusselt numbers have a negative value which decreases when low non-dimensional frequency soars and then increases as the magnitude of f goes up, but in high value of non-dimensional frequency ($f = 150$) the Nusselt numbers dwindle again. On the other hand, the time-averaged heat transfer through the wall is an increasing function of f.

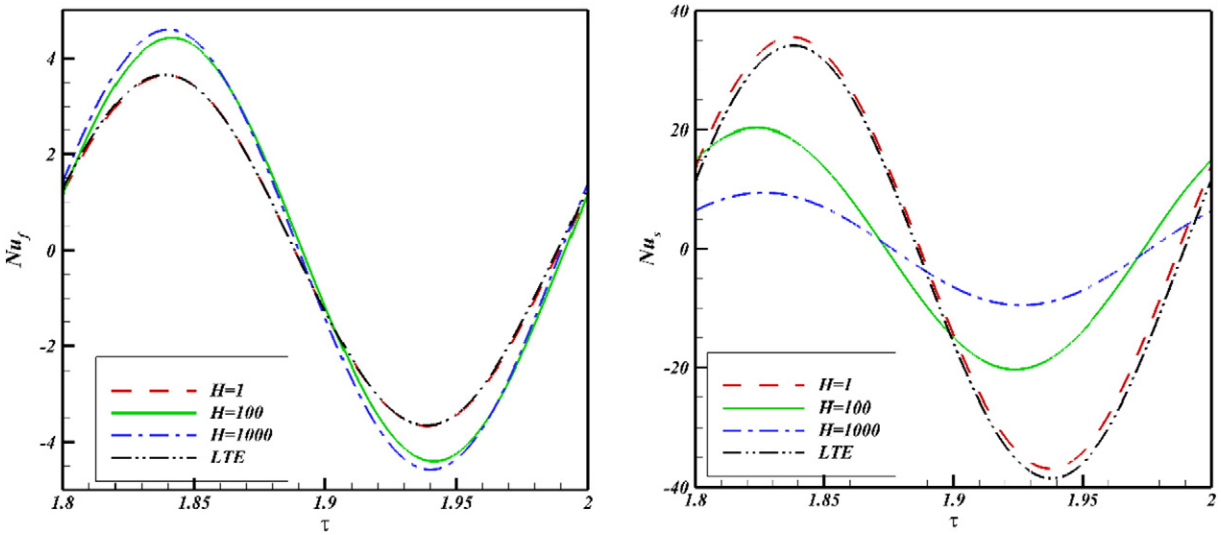

Fig. 14. The effect of parameter H on fluid (left) and solid (right) Nusselt numbers of the left wall; $Ra = 10^3$, $R_k = 0.1$, $f = 10\pi$, $K_r = 100$, $D = 0.1$.

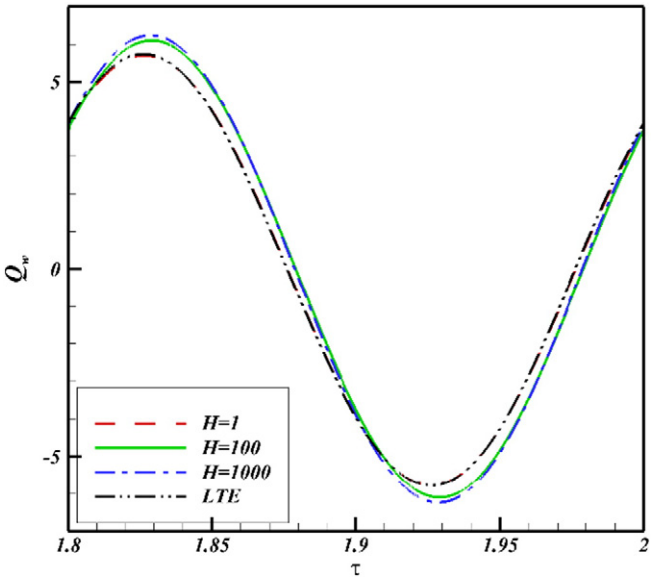

Fig. 15. The effect of parameter H on heat transfer through the left wall; $Ra = 10^3$, $R_k = 0.1$, $f = 10\pi$, $K_r = 100$, $D = 0.1$.

Table 1
The variation of time-averaged Nusselt numbers and heat transfer through the walls with dimensionless frequency.

f	$\overline{Nu}_f$	$\overline{Nu}_s$	$\overline{Q}_w$
10	−0.0107	−0.0107	0.521
30	−0.0180	−0.0180	1.000
50	−0.0152	−0.0152	1.277
70	−0.0115	−0.0115	1.447
90	−0.0096	−0.0096	1.679
110	−0.0085	−0.0085	1.941
130	−0.0079	−0.0079	2.018
150	−0.0082	−0.0082	2.248

References

[1] K. Khanafer, K. Vafai, Isothermal surface production and regulation for high heat flux applications utilizing porous inserts, Int. J. Heat Mass Transf. 44 (2001) 2933–2947.
[2] K. Khanafer, K. Vafai, The role of porous media in biomedical engineering as related to magnetic resonance imaging and drug delivery, Heat Mass Transf. 42 (2006) 939–953.
[3] S.A. Khashan, A.M. AlAmiri, I. Pop, Numerical simulation of natural convection heat transfer in porous cavity heated from below using a non-Darcian and thermal non-equilibrium model, Int. J. Heat Mass Transf. 49 (2006) 1039–1049.
[4] K. Khanafer, K. Vafai, Double-diffusive mixed convection in a lid driven enclosure filled with a fluid-saturated porous medium, Numer. Heat Transf. A 42 (2002) 465–486.
[5] A. Amiri, K. Vafai, Analysis of dispersion effects and non-thermal equilibrium, non-Darcian, variable porosity, incompressible flow through porous medium, Int. J. Heat Mass Transf. 37 (1994) 939–954.
[6] A. Amiri, K. Vafai, T.M. Kuzay, Effect of boundary conditions on non-Darcian heat transfer through porous media and experimental comparisons, Numer. Heat Transf. A 27 (1995) 651–664.
[7] A. Amiri, K. Vafai, Transient analysis of incompressible flow through a packed bed, Int. J. Heat Mass Transf. 41 (1998) 4259–4279.
[8] D.A. Nield, A. Bejan, Convection in Porous Media, second ed. Springer-Verlag, NY, 1995.
[9] K. Vafai, Handbook of Porous Media, second ed. Taylor and Francis Group, NY, 2005.
[10] A. Al-Amiri, Natural convection in porous enclosures: the application of the two-energy equation model, Numer. Heat Transf. A 41 (2002) 817–834.
[11] D.B. Ingham, I. Pop (Eds.), Transport Phenomenon in Porous Media, vol. I, Oxford, Pergamon, 1998.
[12] D.B. Ingham, I. Pop (Eds.), Transport Phenomena in Porous Media, vol. III, Elsevier, Oxford, 2005.
[13] I. Pop, D.B. Ingham, Convective Heat Transfer: Mathematical and Computational Modeling of Viscous Fluids and Porous Media, Pergamon, Oxford, 2001.
[14] D.M. Kim, R. Viskanta, Study of the effects of wall conductance on natural convection in differently oriented square cavities, J. Fluid Mech. 144 (1984) 153–176.
[15] D.M. Kim, R. Viskanta, Effect of wall heat conduction on natural convection heat transfer in a square enclosure, J. Heat Transf. 107 (1985) 139–146.
[16] A. AlAmiri, K. Khanafer, I. Pop, Steady-state conjugate natural convection in a fluid-saturated porous cavity, Int. J. Heat Mass Transf. 51 (2008) 4260–4275.
[17] M.A. Sheremet, I. Pop, Conjugate natural convection in a square porous cavity filled by a nanofluid using Buongiorno's mathematical model, Int. J. Heat Mass Transf. 79 (2014) 137–146.
[18] H. Saleh, N.H. Saeid, I. Hashim, Z. Mustafa, Effect of conduction in bottom wall on Darcy-Benard convection in a porous enclosure, Transp. Porous Media 88 (2011) 357–368.
[19] Y. Varol, H. Oztop, A. Koca, Entropy generation due to conjugate natural convection in enclosures bounded by vertical solid walls with different thicknesses, Int. Commun. Heat Mass Transf. 35 (2008) 648–656.
[20] T. Basak, S. Roy, T. Paul, I. Pop, Natural convection in a square cavity filled with a porous medium: effects of various thermal boundary conditions, Int. J. Heat Mass Transf. 49 (2006) 1430–1441.
[21] J.N. Reddy, An Introduction to the Finite Element Method, McGraw-Hill, New York, 1993.
[22] N.H. Saeid, Conjugate natural convection in a porous enclosure sandwiched by finite walls under thermal nonequilibrium conditions, J. Porous Media 11 (2008) 259–275.